available at www.sciencedirect.com

ScienceDirect

journal homepage: www.elsevier.com/locate/agwat

Calculation of non-reactive chemical distribution in surface fertigation

Theodor S. Strelkoff [a,*], *Albert J. Clemmens* [a,1], *Hugo Perea-Estrada* [b,2]

[a] *U.S. Arid-Land Agricultural Research Center, 21881 North Cardon Lane, Maricopa, AZ 85239, United States*
[b] *Mexican Institute of Water Technology (IMTA), Paseo Cuauhnáhuac 8532, Col. Progreso, Jiutepec, Morelos 62550, Mexico*

ARTICLE INFO

Article history:
Accepted 19 July 2006
Published on line 12 September 2006

Keywords:
Surface irrigation
Fertigation
Modeling

ABSTRACT

A simplified Lagrangian-based theory and practical computation of the longitudinal distribution of fertilizer injected into the inflow to a border strip, basin or furrow is presented as an adjunct to an existing surface-irrigation simulation model. The simplification consists primarily in the assumption that the chemicals are non-reactive and move by advection of the flowing water and that no mixing, dispersion, or diffusion of the chemical takes place. In a corollary calculation, the composition of runoff, in terms of water fractions selected for fertilizer injection, is also simulated. Comparisons of calculated post-irrigation longitudinal distribution of infiltrated chemical are made with the results of a complete advection-diffusion model that had already been validated in the field for injection of fertilizer pulses into the furrow inflow.

1. Introduction

To ensure that all the plants in a field receive sufficient fertilizer without excesses that can lead to ground water pollution, the amount applied and its distribution over the cropped area need to be controlled. The convenience and control of fertilizer applied with irrigation water has made fertigation a common technique with pressurized irrigation systems. The method is also used by growers with surface irrigation systems. In this context, it is still easy to control the injection schedule of fertilizer, but difficult to relate the injection timing to the resultant post-irrigation distribution of fertilizer in the field. Thus, it is difficult to make recommendations on whether to apply fertilizer during the entire irrigation period, or during selected fractions of it, e.g., the first half, or middle third, or in pulses, etc.

Subject to some significant assumptions, a simple addition to the existing surface irrigation simulation software, SRFR (Strelkoff et al., 1998), allows calculation of the ultimate longitudinal distribution of chemical consequent to any trial injection schedule. This allows playing a number of what-if scenarios in the search for an optimum. Assuming that at the point of injection the chemical is uniformly mixed across the area of flow, and remains identified with the water into which it was injected, the volume of irrigation-water inflow is divided into a selected number of fractions, and the ultimate longitudinal distribution of infiltrated depth from each of the fractions is calculated. The distribution of infiltrated chemical is then the same as that of the water fraction into which it was injected.

The theory governing the tracking of the fractions of applied water is based on the assumption that no mixing takes

* *Corresponding author*. Tel.: +1 520 316 6382; fax: +1 520 316 6330.
E-mail addresses: fstrelkoff@uswcl.ars.ag.gov (T.S. Strelkoff), bclemmens@uswcl.ars.ag.gov (A.J. Clemmens), hpe650820@gmail.com (H. Perea-Estrada).
[1] Tel.: +1 520 316 6373; fax: +1 520 316 6330.
[2] Tel.: +52 777 329 3600x609; fax: +52 777 329 3657.
0378-3774/$ – see front matter
doi:10.1016/j.agwat.2006.07.006

place between the fractions. Fractions released earlier into the surface flow are assumed to move down the flow channel ahead of fractions released later; impenetrable walls, moving at the average water velocity at the particular cross section, are assumed between the fractions. The downstream-most fraction, if it gets to the end of the flow channel, either runs off, or piles up against a check, to a depth determined by the stream-simulation part of SRFR, until it has all either runoff or infiltrated. SRFR expresses mass and momentum conservation in a series of water-filled cells with boundaries $k = 1, 2, 3, \ldots, N$, solves the resulting equations for depth and discharge at all k over a sequence of computational time steps, and so predicts the water surface profile as it evolves over time.

Assuming uniform flow velocity along a furrow, Boldt et al. (1994) developed a similar procedure (SIFUM—Surge Irrigation Fertigation Uniformity Model) for utilizing files generated by an early version of the surface-irrigation software, SIRMOD (Surface Irrigation Model, Walker, 2003). Sabillon and Merkley (2004) developed a stand-alone model that in an implicit numerical scheme solves the partial differential equations of continuity, momentum, and fertilizer mass balance in a purely advective context, with diffusion limited to numerical sources. Perea-Estrada (2005) solved an advection-diffusion equation using a split operator approach to deal with the advection and dispersion aspects of the fertilizer transport sequentially at each time step, rather than simultaneously. To avoid numerical diffusion in the advection calculation, Perea-Estrada employed a method of characteristics, with the inverse slopes of the characteristic curves equal to local water velocity. Cubic-spline interpolation allowed him to determine fertilizer concentration on a particular segment of a characteristic curve with accuracy (see also Strelkoff and Sakkas, 1974; Katopodes and Strelkoff, 1977; Strelkoff and Clemmens, 2006, for other examples of characteristics in simulating surface irrigation). The calculation of turbulent diffusion was performed for each time and space node by the Crank–Nicholson scheme. The coefficient of longitudinal dispersion was calculated by the Fischer equation (Eq. (5.19) in Fischer et al., 1979) for flows with substantial velocity variation in a cross section, both laterally and vertically. Below, results of the proposed simple, advective numerical scheme are compared with Perea-Estrada's results. The comparison suggests that in the advection-dominant case of furrow flow, useful results are obtained with the simple method proposed.

2. Qualitative considerations

Fig. 1 illustrates the surface and infiltrated volumes of water after the first two fractions have been released. Fig. 1(a) represents time $T_{①}$ when all of fraction 1 has been released and fraction 2 is about to enter the field. Fig. 1(b) refers to time $T_{②}$, when all of fraction 2 is on the field, and fraction 3 is just about to enter. With a constant inflow rate and equal fractions, $T_{②} = 2T_{①}$. The y-axis represents surface-water depth and the z-axis, the infiltrated depth, while x is distance down the field. The encircled numbers identify the origin of the various portions of surface and infiltrated water. The heavy vertical line represents the impenetrable wall separating the surface

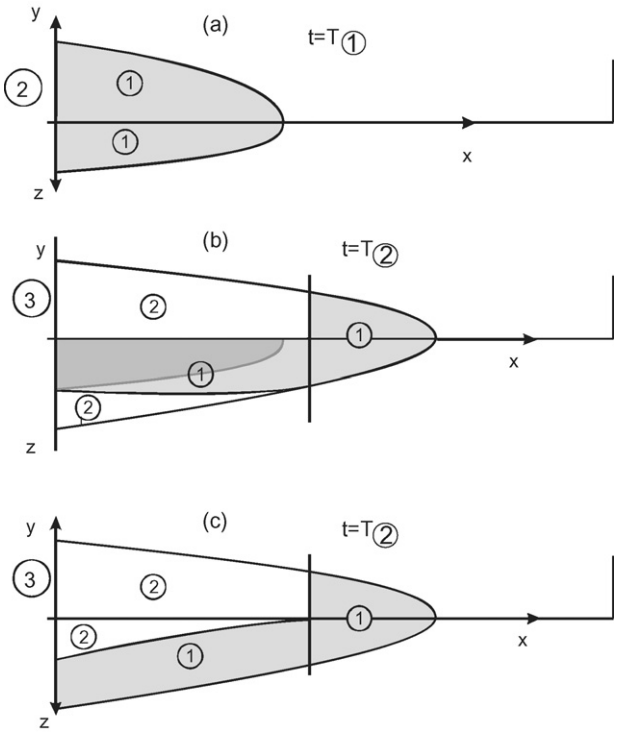

Fig. 1 – Distribution of surface and infiltrated waters from two inflowing fractions. Surface depth: y; infiltrated depth: z; distance from upstream end: x. (a) Fraction 1 is wholly on the field; fraction 2 about to enter, (b) fraction 2 wholly on field; fraction 3 ready to enter and (c) same as (b), but first infiltrated fraction is plotted below second infiltrated fraction.

water fractions 1 and 2. In Fig. 1(b), infiltrated water depths from fraction 1 are found on both sides of the wall. The darker shaded area represents the infiltrated water from fraction 1 at time $T_{①}$. Additional infiltration of 1-water occurs in the time interval between $T_{①}$ and $T_{②}$ on the downstream side of the wall as it moves downstream during that period. The heavy line in the figure separates infiltrated 1-water (lightly shaded) from 2-water (not shaded) infiltrated in the same time period. The vertical distances between the curves represent merely the volume per unit field area (depth) of infiltration of the various components; the curves are not intended to imply the location in the soil profile of these fractions—fraction 2-water is not below fraction 1-water. Part (c) of the figure, on the other hand, represents the same physical situation as part (b), except that infiltrated 1-water has been plotted below the infiltrated 2-water to illustrate the consequences of an additional assumption that water infiltrated earlier at some point in a furrow proceeds downward through the soil ahead of water infiltrated later. This assumption is not needed, if the purpose of the calculations is to determine the post-irrigation longitudinal uniformity of the fertilizer application. It plays a role only if one is concerned about the fate of the fertilizer once it has entered the soil, e.g., whether it lies within the root zone for crop uptake, or below the root zone, on its way toward the groundwater, etc.

3. Mass balances

Fig. 2 illustrates the stream lengths of surface-water fractions at two arbitrary times, t_A and t_B, during the irrigation (with $t_B > t_A$). A number of SRFR time steps have elapsed between t_A and t_B. Infiltrated depths are not shown here. The light vertical lines are the computational cell boundaries in SRFR's solution grid. The dotted vertical lines are explained further on. The heavy vertical lines are, again, the nominal boundaries between the various water fractions at the end of the pertinent time step. Each fraction consists, typically, of a number of SRFR cells and is labeled by the order in which it was released into the field, 1, 2 and so on, up eventually to N_F, the total number of fractions into which the inflow volume is divided (user-selectable in SRFR). Each fraction in contact with the soil surface infiltrates its water into the soil directly below (as in Fig. 1). During the course of a time step, infiltration from the mth fraction takes place from the portion of the surface stream contained between the bounding k values for that fraction (k being the distance step index, as in Fig. 2). At the end of any SRFR time step, the accumulated depth of infiltration $z_{mk,2}$ at a k value lying within the set associated with m is given by:

$$z_{mk,2} = z_{mk,1} + \frac{A_{zk,2} - A_{zk,1}}{W} \quad (1)$$

in which, the subscripts 1 and 2 correspond to the beginning and end of the time step, respectively, the A_z are the volumes infiltrated per unit length of channel (a dependent simulation variable calculated by SRFR) and W is the representative width associated with the flow channel, relating the field depth of infiltration to the volume infiltrated per unit length of channel. It is apparent from Eq. (1) that the principal task in keeping track of the depths z_m of infiltrated m-water consists in tracking the boundaries between the fractions.

The impenetrable interfaces move downstream and closer together as the surface water between them is used up in infiltration. The movement of the most downstream one, furthermore, is accelerated by any runoff. Initially, $m = 1$, i.e., only 1-water has entered the field, and there is as yet no interface with 2-water. Once the total volume of 1-water, V_{Q1}, has entered the field, 2-water follows on its heels. The location of the interface between them is found through a fraction-by-fraction mass balance, pertinent at every subsequent time level of the simulation:

$$V_{Q_m} = V_{Z_m} + V_{RO_m} + V_{Y_m} \quad (2)$$

in which, in the case of equal sized fractions, $V_{Q_m} = V_{Q_{HYD}}/N_F$ ($V_{Q_{HYD}}$ is the total volume represented by the inflow hydrograph). As noted, V_{Q_m} is user selectable, e.g., to correspond to pulses of injected fertilizer as in the example below. V_{Z_m} is the current infiltrated volume of fraction m, V_{RO_m} is the current runoff volume of m-water, and V_{Y_m} is the current volume of m-water remaining on the surface. The interface location is implicit in the infiltrated-volume and surface-volume calculations, since, at any given time level, there will be just one location along the length of the flow channel at which Eq. (2) will be satisfied for each water fraction on the field. The dotted vertical lines in Fig. 2 represent those non-grid x-values at which calculated sums of surface, infiltrated, and runoff volumes (from 2-water, for the example in Fig. 2) would exactly equal the volume of 2-water released. For computational simplicity, the boundaries of the fractions, theoretically located in the interior of a cell, are nominally placed at the nearest downstream cell boundary. The finer is the SRFR grid, the smaller are the cells and the closer is this approximation.

The calculations in SRFR proceed cell by cell going upstream, starting from the downstream-most cell. That cell contains water of fraction, m_{min}, by definition the earliest-released fraction still on the field—all water fractions identified by smaller m have, by this time, either infiltrated or run off or both (initially, of course, $m_{min} = 1$). In the progress of calculations from downstream to upstream, when at a cell the sum of surface water, infiltration, and runoff volumes associated with a particular fraction m (i.e., the totals calculated for all cells from the impenetrable interface downstream, up to and including the current cell) exceeds the given volume of the fraction, the cell-index of the nominal upstream bounding interface is given by the k on the downstream side of the cell (the dotted line in Fig. 2(b) illustrates the passage of m_{min} from 2 to 3). It follows that the infiltration increment from that cell is attributed to the next fraction released, $m + 1$, as is the increment of surface water in that cell, thus incurring a small error in the identity of water particles, but not influencing the total volume balance. At any time level, the infiltration and volume calculations start at $k = N$ and end at $k = 1$ (N, under the name N_{ZP2}, is a SRFR simulation variable, the total number of cell boundaries at the end of a time step). In effect, then, at every time level, every k is associated with one or another value of m.

Of note, it is possible, in principle, to use up a fraction, m, from the surface stream while $m + 1$ and $m - 1$ are still on the surface.

Ultimately, after all applied water has receded from the soil, the z_m values accumulated under Eq. (1) constitute the distances between adjacent plotted post-irrigation fertigation profiles (illustrated further on as Figs. 4–10).

A flow chart schematic of the fertigation-distribution computations undertaken at the end of every SRFR-simulation

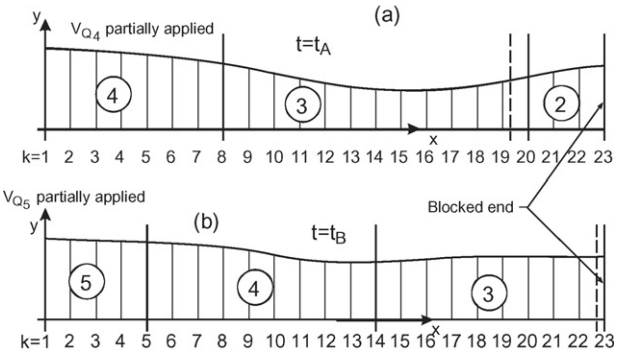

Fig. 2 – Partitioning of inflow into fractions at two times, t_A and t_B ($t_B > t_A$). k: SRFR cell boundaries for simulation of irrigation. Encircled numbers: sequence of released inflow fractions. Dotted lines: location of boundaries between fractions with exact volume balance. Solid lines: nominal boundaries between fractions.

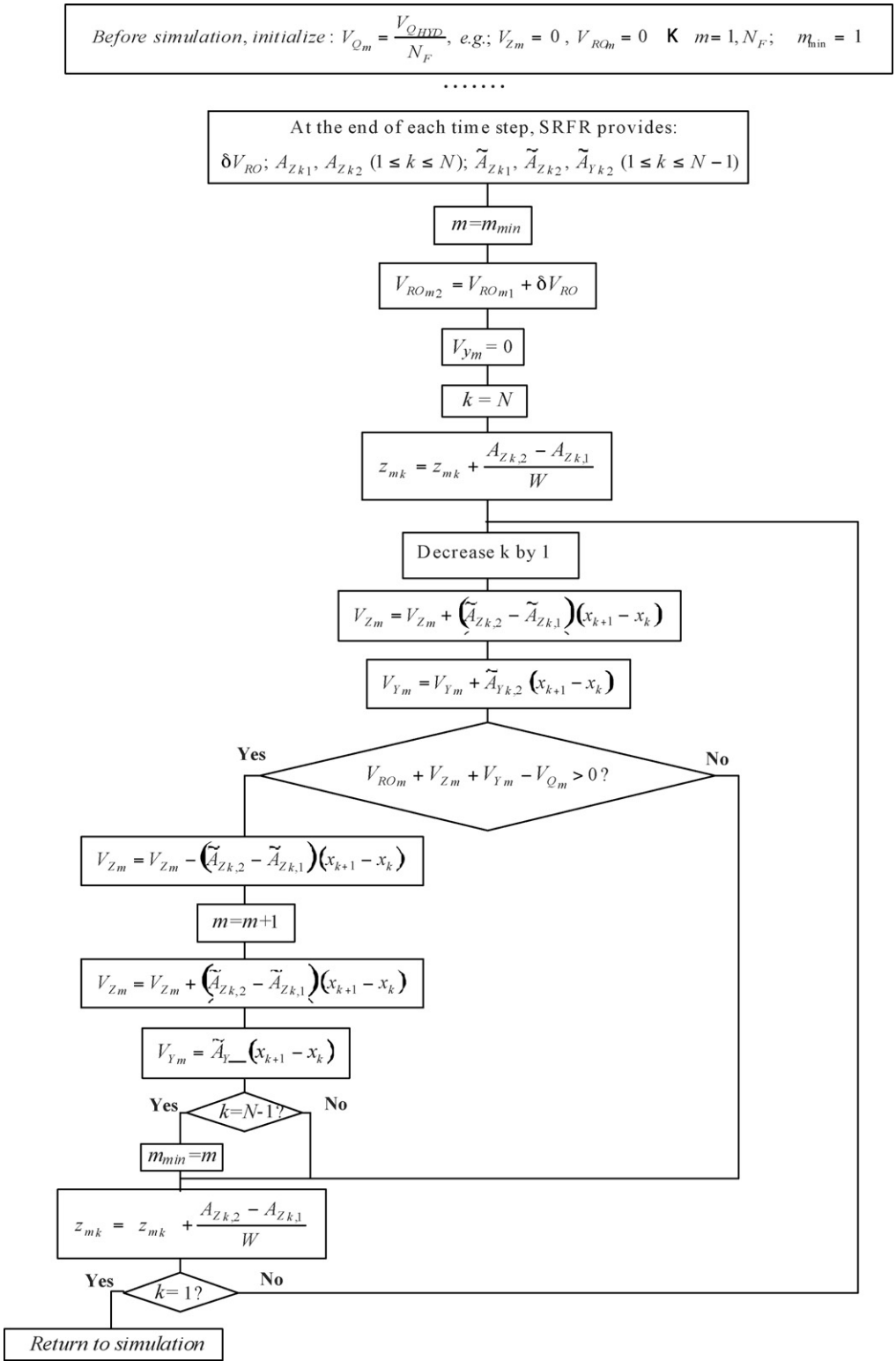

Fig. 3 – Flow chart for fertigation-distribution computations.

time step is depicted in Fig. 3 (certain variables are, as noted, initialized prior to the first step of simulation). In the flow chart, it should be noted that the equal sign (=) represents a replacement of value, rather than an algebraic equality. The quantity δV_{RO} is the increment of runoff incurred over the time step. $\tilde{A}_Z$ and $\tilde{A}_Y$ are, respectively, the average infiltrated volume per unit length over one grid cell, and average cross sectional area of flow in a cell (surface volume per unit length). Subscripts 1 and 2 represent, respectively, the beginning and end of a time step. It is seen that most of the computation is

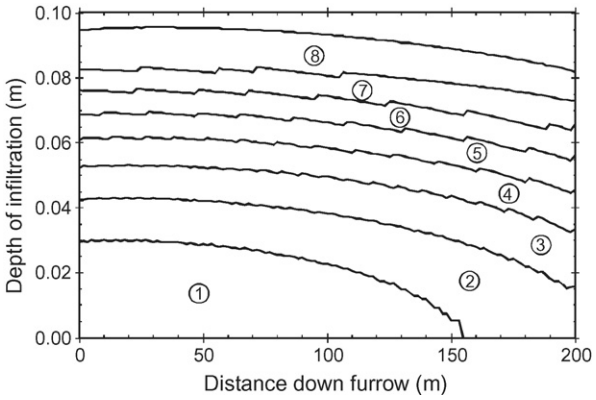

Fig. 4 – Post-irrigation longitudinal distribution of eight water fractions. Vertical distance between neighboring fractions is the depth of that fraction. Open ended sloping furrows. Advance time = 97 min; cutoff at 240 min.

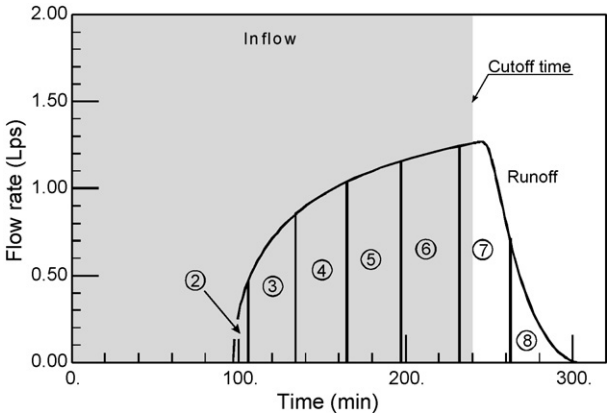

Fig. 5 – Water fractions identified in runoff hydrograph; cutoff at 240 min. Inflow hydrograph is shown (gray scale) for comparison.

devoted to partitioning the surface stream into segments identified by the *m*-water of which they are constituted. The segments consist of those cells that contributed to the infiltration of *m*-water during the previous time step. In the process, the infiltration profiles of *m*-water are updated. As a potential convenience to the reader with a local simulation program who might wish to insert therein the pertinent statements, the Fortran code corresponding to these computations is available from the senior author upon request.

4. Sample applications

Figs. 4–10 illustrate the distribution of eight equal inflow fractions in the infiltrated water and runoff under a variety of scenarios. Again, the distance between infiltration curves represents the depth of infiltration of a particular fraction. Of note, the coordinates of the curves are recorded (in SI units) in an output text file produced in every SRFR simulation. These files are read by SRFR itself to plot output data as requested by the user, but they also remain on disk for any other calculations a user may require.

In the runs illustrated in Figs. 4–8, the flow channels are 200 m long trapezoidal furrows with bottom width of 250 mm, side slopes 1 on 1, and set 1 m apart on a slope of 0.0004. Infiltration is calculated by the Kostiakov power law, $k\tau^a$, with τ infiltration time, $k = 42.85$ mm/h^a, and $a = 0.526$, and a nominal wetted perimeter equal to the furrow spacing; Manning $n = 0.04$. The inflow rate in each case is 2 L/s, leading to an advance time (to reach field end) of 97 min. For Fig. 9, all conditions are the same except that the furrow is level, with an advance time of 108 min.

Fig. 4 is for an open-ended furrow. Cutoff is at 240 min. Evidently, water from fraction 1 never reaches the portion of the field beyond 155 m. The distribution from fraction 2 extends over the entire length of run (as do all subsequent fractions), the depth rising gradually to a peak at 155 m, with a subsequent decrease over the remaining 45 m. Fig. 5, showing the fractions as they supercede one another in the runoff hydrograph, is derived from the aforementioned SRFR-output

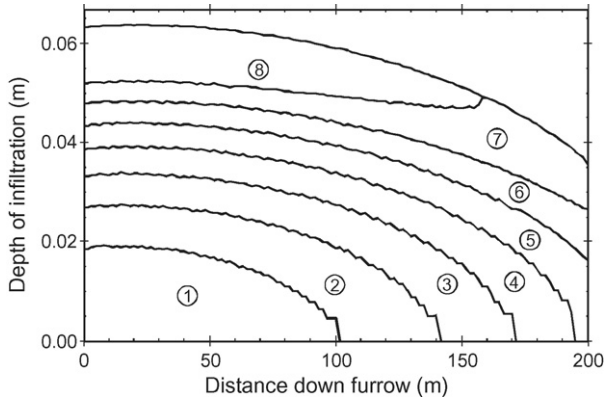

Fig. 6 – Post-irrigation longitudinal distribution of eight water fractions. Vertical distance between neighboring fractions is the depth of that fraction. Open ended sloping furrows. Advance time = 97 min; cutoff at 100 min.

text file. If the chemical composition of runoff destined for reuse or off-site discharge is of interest, the volumes associated with each fraction can play a role in selecting those in which to inject the fertilizer.

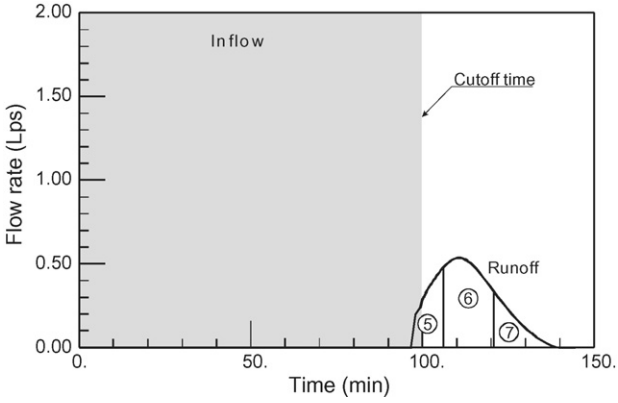

Fig. 7 – Water fractions identified in runoff hydrograph; cutoff at 100 min. Inflow hydrograph is shown (gray scale) for comparison.

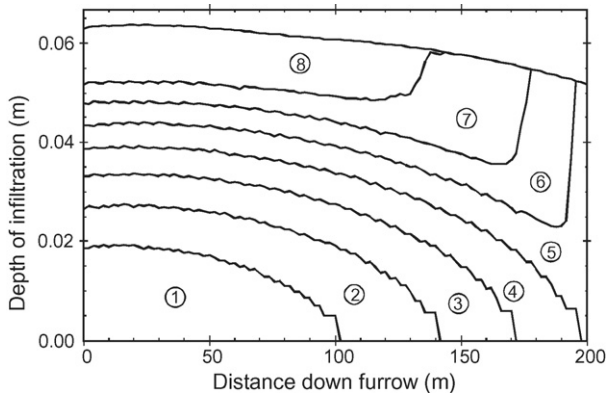

Fig. 8 – Post-irrigation longitudinal distribution of eight water fractions. Vertical distance between neighboring fractions is the depth of that fraction. Closed-end sloping furrows. Advance time = 97 min; cutoff at 100 min.

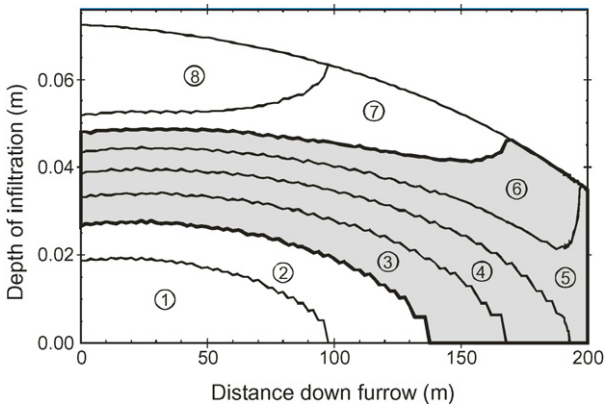

Fig. 9 – Post-irrigation longitudinal distribution of eight water fractions. Vertical distance between neighboring fractions is the depth of that fraction. Closed-end level furrows. Advance time = 108 min; cutoff at 100 min.

Fig. 6 is for the same furrow conditions, but with inflow cutoff at 100 min—note the scale difference with Fig. 4. It is of interest that the last fraction to enter the furrow as well as the first and second do not reach the end. Fig. 7 shows the runoff composed of the various fractions in this case.

In Fig. 8, the sloping furrow is blocked to prevent outflow, with all else the same. In Fig. 9, the blocked furrow is level. Not surprisingly, the blocked ends yield distributions markedly different from those with a free outflow, as the early fractions are ponded on the surface at the downstream end. There are significant differences, as well, between the level (Fig. 9) and sloping (Fig. 8) blocked furrows. The early fractions are distributed in about the same way, but the sixth, seventh, and eighth fractions in the sloping case are pushed downstream and have greater magnitudes. These phenomena have significant implications for fertigation strategies; for example in Fig. 9, the longitudinal infiltration profile of the middle half of the inflow is given by the vertical distance in the shaded area between the two heavy black curves.

The simulations described were run with fine grids to minimize the coarseness of the resolution stemming from the aforementioned nominal interface between m and $m + 1$ water.

Sometimes, the cumulative-infiltration formula is characterized by a significant constant term, typical of cracked clay soils. Then, the infiltration profile possesses a discontinuous step front, reflecting the essentially instantaneous infiltration of some depth as soon as the water is made available at the surface. In this case, the SRFR-output text file is augmented with rows of data providing a second ordinate (zero depth) at each x-value marking the advancing surface-stream front. This allows the plot to exhibit the correct discontinuous infiltration-profile front without affecting the plotting of the remaining fractions. Fig. 10 is for a 180 m-long blocked-end basin 4.5 m wide, with Manning $n = 0.04$ set on a slope of 0.0008. Infiltration is characterized by a Modified Kostiakov formula, $k\tau^a + b\tau + c$, with $k = 13$ mm/h^a, $a = 0.43$, $b = 15.5$ mm/h and $c = 20$ mm. The inflow rate is 6.55 L/s for 180 min (advance time is 160 min). The four identified fractions of inflow lead to the profiles shown.

The three sets of curves show the effect of variable cell size on the profiles, with grids of 20, 80 and 140 cells featured. A coarse grid with the proposed stair-step approach to determining the boundaries of the fractions can cause an earlier water fraction to be misidentified as a later fraction, as in the first quarter volume in Fig. 10, or artificially moved upstream, as in the third quarter fraction. These errors are significantly reduced by employing a finer grid in the SRFR simulation. At the same time, while a 20-cell grid may well be too coarse, little improvement is seen for this example in going from 80 to 140 grid cells. In any event, the procedures outlined do not influence the ultimate distribution of water—only its partitioning amongst the fractions. Inasmuch as alternate fractions could be carrying a constituent, such as fertilizer solute described in the next section, these numerical errors would affect the ultimate longitudinal distribution. Noting the mass error, reflected in the difference between fertilizer injected, infiltrated, and run off, allows a user to assess the magnitude of the impact.

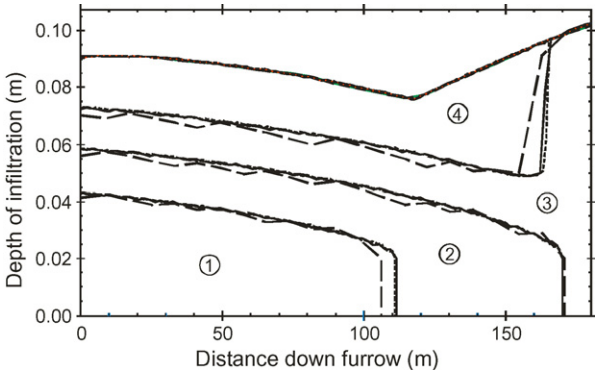

Fig. 10 – Effect of solution grid on post-irrigation longitudinal distribution of four source fractions. Closed-end sloping basin. Advance time = 160 min; cutoff at 180 min. Dashed curve: 20 cells; solid curve: 80 cells; dotted curve: 140 cells.

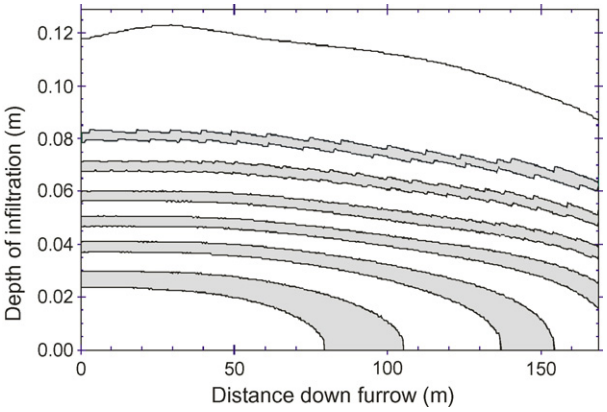

Fig. 11 – Infiltration of successive water fractions controlled by pulses of injected fertilizer. Open-ended furrow, #1 in MAC field experiments.

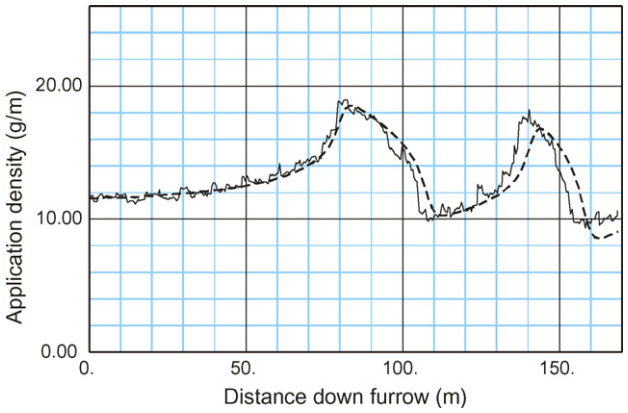

Fig. 12 – Post-irrigation distribution of mass per unit length in open-ended furrow, #1. Comparison of proposed simplified model and solution of ADE partial differential equation. Solid line: proposed advection solution; dashed line: advection-diffusion model (Perea-Estrada, 2005) with longitudinal diffusion coefficient given by Fischer formula.

5. Application to pulse fertigation. Model verification

As pointed out by Walker (2004), the simple addition of a concentration term to the computations allows the prospective user to see the impact of various injection timings on the ultimate mass distribution of a non-reactive chemical (be it fertilizer, pesticide or herbicide). Fig. 11 (free-draining furrow) and Fig. 13 (blocked-end furrow) illustrate the infiltration profiles of water fractions determined by the timing of pulses of fertilizer injected into the furrow irrigation water. As described in Perea-Estrada (2005), a program of tracer-concentration measurements in a field experiment at the University of Arizona, Maricopa Agricultural Center (MAC), served to verify the predictions of a model based on solution of the advection-diffusion equation (ADE). Input data for the ADE solution comprised SRFR-simulated depths and velocities. In the open furrow, #1 in the experiments, the pulses of fertilizer were injected in accord with Table 1. Fertilizer-tank concentration remained constant at 247.4 g/L. The high concentration was chosen to ensure that even after dilution in the furrow flow, the tracer would be measurable over the peaks and hollows of the hydrographs as they swept downstream. Fig. 11 shows the infiltration contributed by each fraction of water—those containing tracer are shaded. Fig. 12 gives the post-irrigation distribution of infiltrated chemical (g/m). This represents the contributions of all the shaded areas of Fig. 11, which in this case, were all at the same concentration C, since the injection rate Q_{PULSE} was the same for each pulse, and the average inflow rate $\bar{Q}_{IN}$ was assumed the same for all fractions in calculating the (unequal) fraction volumes (in fact, the measured instantaneous rate varied a little in the field; this was mirrored in the ADE solution). Indeed:

$$C_m \cong \frac{Q_{PULSE_m} C_{TANK}}{60\bar{Q}_{IN}} = \frac{C_{TANK} Q_{PULSE_m} (T_{END\,PULSE_m} - T_{BEGIN\,PULSE_m})}{V_{Q_m}} \quad (3)$$

the approximation becoming ever more exact as the injection flow rate is much smaller than the furrow inflow. Thus, an ordinate in Fig. 12 is calculated by summing up the segments of shaded ordinates from bottom to top in Fig. 11, weighted by the concentration in each segment. The peaks and valleys in Fig. 12 are the result of the timing and length of pulse applications, time variations in infiltration, and potentially, variations in concentration at each injection. The major part of the first peak in Fig. 12, at about 80 m, reflects the large ordinate in the first shaded water fraction at 80 m in Fig. 11, while the peak at around 140 m reflects the large ordinate there in the second shaded fraction in Fig. 11.

The essential features of the field-validated ADE solution are duplicated by the proposed simplified model in this advection dominated case. The mild effects of turbulent dispersion are evident in the downstream portions, where the second peak in particular is somewhat delayed and reduced.

Table 1 – Fertigation pulse history: furrow #1—open end

Begin pulse (min)	End pulse (min)	Injection rate (mL/min)
15	25	190
40	50	190
65	75	190
90	100	190
115	125	190
140	150	190

Table 2 – Fertigation pulse history: furrow #4—closed end

Begin pulse (min)	End pulse (min)	Injection rate (mL/min)
15	25	180
40	50	180
65	75	180
86	96	180
111	121	180

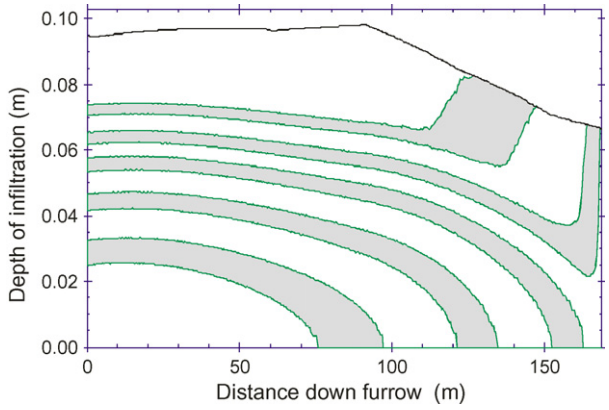

Fig. 13 – Infiltration of successive water fractions controlled by pulses of injected fertilizer. Blocked-ended furrow, #4 in MAC field experiments.

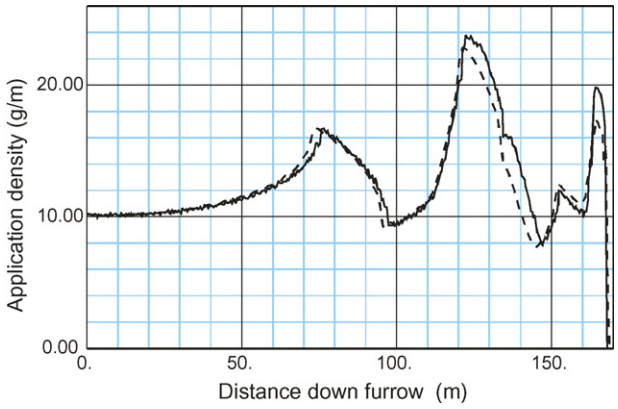

Fig. 15 – Post-irrigation distribution of mass per unit length in blocked furrow, #4. Comparison of proposed simplified model and solution of ADE partial differential equation without dispersion. Solid line: proposed advection solution; dashed line: advection-diffusion model (Perea-Estrada, 2005), with longitudinal dispersion coefficient set to 0.

As noted above, the longitudinal dispersion coefficient in the ADE was calculated by the Fischer et al. (1979) formula for the hydraulic conditions at each point in space and time, with a typical value at about 1 m^2/min.

Fertigation in a blocked-end furrow (furrow #4 in the MAC field experiments) is presented in Figs. 13 and 14, for which the injection details are given in Table 2. In this case, the tank concentration was 240.8 g/L. The peaks in Fig. 14 are more extreme and varied, because the infiltration of the pertinent (loaded) fractions is more extreme and varied in the blocked-end case (see Fig. 13).

The details of the effects of longitudinal dispersion are more pronounced than in the free-draining case, though the overall pattern of distribution as calculated by the proposed simplified model in Fig. 14 agrees with the ADE model results. That the differences in solutions are attributable to longitudinal dispersion is made clear in Fig. 15, for which the ADE equation was solved in a purely advective context, with the longitudinal dispersion coefficient set to 0. Of note, the mass error in the simplified calculation is very small, with 2.167 kg injected, determined by monitoring the injection schedule, and 2.164 kg infiltrated, calculated by integrating the application density over the length. In the open-end case, the mass carried in the tail water needs to be included in the balance.

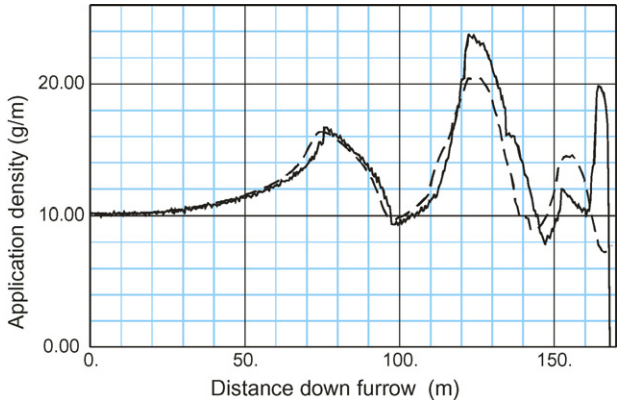

Fig. 14 – Post-irrigation distribution of mass per unit length in blocked furrow, #4. Comparison of proposed simplified model and solution of ADE partial differential equation. Solid line: proposed advection solution; dashed line: advection-diffusion model (Perea-Estrada, 2005), with longitudinal diffusion coefficient given by Fischer formula.

6. Conclusions

A simple scheme coupled to an existing surface irrigation simulation model has been proposed for tracking the successive fractions of inflowing water as they infiltrate into the soil surface or run off downstream. When fertilizer is injected into selected fractions in fertigation, such a simulation can be used to predict the post-irrigation longitudinal distribution of fertilizer as well as the discharge of fertilizer in the runoff stream. The main assumption in the model is that there is no mixing of the water fractions, and that the chemical remains with the water into which it was injected. The origins of the model are clearly Lagrangian, for as coarse as the analysis is, the individual fractions of water are in fact tracked during the irrigation. As such, the approach inherently avoids numerical diffusion. Numerical error in the distribution of fertilizer from the individual fractions can be monitored by checking the mass balance after the irrigation is complete.

Acknowledgements

The writers are grateful to Floyd Adamsen and Douglas Hunsaker of the U.S. Arid-Lands Agricultural Research Center for their assistance in planning and running the field tracer experiments used in validating the Perea-Estrada advection-diffusion model, which was then used herein for comparison with the simplified solution in Figs. 12, 14 and 15.

REFERENCES

Boldt, A.L., Watts, D.G., Eisenhauer, D.E., Schepers, J.S., 1994. Simulation of water applied nitrogen distribution under surge irrigation. Trans. ASAE 37, 1157–1165.

Fischer, H.B., Imberger, J., List, J.E., Koh, R.C.Y., Brooks, N.H., 1979. Mixing in Inland and Coastal Waters. Academic Press Inc., New York, NY.

Katopodes, N.D., Strelkoff, T., 1977. Hydrodynamics of border irrigation – Complete model. J. Irrig. Drain. Eng. ASCE 103, 309–324.

Perea-Estrada, H., 2005. Development, verification and evaluation of a solute transport model in surface irrigation. Ph.D. Dissertation. Department of Agricultural and Biosystems Engineering, The University of Arizona, Tucson, AZ.

Sabillon, G.N., Merkley, G.P., 2004. Fertigation guidelines for furrow irrigation. Spanish J. Agric. Res. 2, 576–587.

Strelkoff, T.S., Clemmens, A.J., Schmidt, B.V., 1998. SRFR, Version 3.31—A Model for Simulating Surface Irrigation in Borders, Basins and Furrows. U.S. Arid-Lands Agricultural Research Center, USDA/ARS, 21881 N. Cardon Lane, Maricopa, AZ.

Strelkoff, T.S., Sakkas, J.G., 1974. Hydrodynamics of surface irrigation—advance phase. J. Irrig. Drain. Eng. ASCE 100, 31–48.

Strelkoff, T.S., Clemmens, A.J., 2006. Hydraulics of surface systems. In: Hoffman, G.J., Evans, R.G., Jensen, M.E., Martin, D.L., Elliott, R.L. (Eds.), Design and Operation of On Farm Irrigation Systems, second ed. (Chapter 13), ASABE Special Monograph, in press.

Walker, W.R., 2003. SIRMOD—Surface Irrigation Simulation, Evaluation and Design. User's Guide and Technical Documentation. Biological and Irrigation Engineering, Utah State University, Logan, Utah, 63 p.

Walker, W.R., 2004. Personal communication.